Accepted Manuscript

Improved leakage current properties of ZrO2/(Ta/Nb)Ox-Al2O3/ZrO2 nanolaminate insulating stacks for dynamic random access memory capacitors

Takashi Onaya, Toshihide Nabatame, Tomomi Sawada, Kazunori Kurishima, Naomi Sawamoto, Akihiko Ohi, Toyohiro Chikyow, Atsushi Ogura

PII: S0040-6090(18)30089-0
DOI: https://doi.org/10.1016/j.tsf.2018.02.010
Reference: TSF 36472

To appear in: *Thin Solid Films*

Received date: 8 December 2016
Revised date: 22 December 2017
Accepted date: 5 February 2018

Please cite this article as: Takashi Onaya, Toshihide Nabatame, Tomomi Sawada, Kazunori Kurishima, Naomi Sawamoto, Akihiko Ohi, Toyohiro Chikyow, Atsushi Ogura , Improved leakage current properties of ZrO2/(Ta/Nb)Ox-Al2O3/ZrO2 nanolaminate insulating stacks for dynamic random access memory capacitors. The address for the corresponding author was captured as affiliation for all authors. Please check if appropriate. Tsf(2017), https://doi.org/10.1016/j.tsf.2018.02.010

Improved leakage current properties of $ZrO_2/(Ta/Nb)O_x$-Al_2O_3/ZrO_2 nanolaminate insulating stacks for dynamic random access memory capacitors

Takashi Onaya[a, b, *], Toshihide Nabatame[b, c], Tomomi Sawada[b, c], Kazunori Kurishima[a, b], Naomi Sawamoto[a], Akihiko Ohi[b], Toyohiro Chikyow[b], Atsushi Ogura[a]

[a] Department of Electrical Engineering, Graduate School of Science and Technology, Meiji University, 1-1-1 Higashimita, Tama-ku, Kawasaki, Kanagawa 214-8571, Japan

[b] International Center for Materials Nanoarchitectonics (WPI-MANA), National Institute for Materials Science (NIMS), 1-1 Namiki, Tsukuba, Ibaraki 305-0044, Japan

[c] CREST, Japan Science and Technology Agency (JST), 4-1-8 Honcho, Kawaguchi, Saitama 332-0012, Japan

Corresponding author: Department of Electrical Engineering, Graduate School of Science and Technology, Meiji University, 1-1-1 Higashimita, Tama-ku, Kawasaki, Kanagawa 214-8571, Japan

Tel./Fax: +81 44 934 7352

International Center for Materials Nanoarchitectonics (WPI-MANA), National Institute for Materials Science (NIMS), 1-1 Namiki, Tsukuba, Ibaraki 305-0044, Japan

Tel.: +81 29 851 3354; Fax: +81 29 860 4916

E-mail address: ce61020@meiji.ac.jp, ONAYA.Takashi@nims.go.jp

Abstract

The influence of amorphous high-*k* interlayers, such as Al_2O_3, $(Ta/Nb)O_x$ (TN), and $(Ta/Nb)O_x$-Al_2O_3 (TNA), on the leakage current (*J*) and dielectric constant (*k*) for metal-insulator-metal capacitors with ZrO_2/high-*k*/ZrO_2 nanolaminate insulating films and TiN electrodes was investigated. The insulating films were prepared by atomic layer deposition followed by post-deposition annealing at 600°C. The capacitance equivalent thickness (CET) of the capacitors increased in the order $ZrO_2/(Ta/Nb)O_x/ZrO_2$ (ZTNZ) < $ZrO_2/(Ta/Nb)O_x$-Al_2O_3/ZrO_2 (ZTNAZ) < $ZrO_2/Al_2O_3/ZrO_2$ (ZAZ), owing to the *k* values for Al_2O_3 (~6), TNA (~9), and TN (~11). The *J* values at 0.6 V for capacitors with a CET of 1.1 nm increased in the order ZTNAZ < ZAZ << ZTNZ. The effect of a high-*k* interlayer on the *J* characteristics appeared above a thickness of 0.4 nm in the case of Al_2O_3 and TNA, while a 0.8-nm-thick TN maintained high *J* values. Based on these results, there are three important factors as a high-*k* interlayer to reduce *J* value, such as a band gap larger than that for TN (4.4 eV), a thickness of ≥ 0.4 nm, and an amorphous structure. Therefore, to achieve the low *J* and CET, TNA is a promising candidate material for a high-*k* interlayer for future dynamic random access memory.

1. Introduction

High-dielectric-constant (high-*k*) materials have been widely investigated as a gate insulator for metal-oxide-semiconductor field effective transistors (MOSFETs), a storage cell for flash memory, an active layer for resistive random access memory (ReRAM) and memristors, a channel layer for oxide thin film transistors (oxide-TFTs), and an insulator for dynamic random access memory (DRAM) [1-11]. Among the high-*k* materials investigated, HfO_2 [12-14], Ta_2O_5 [15-17], Nb_2O_5 [17], $SrTiO_3$ [18-20], TiO_2 [20-23], and ZrO_2 [18, 24-33] have recently attracted much interest for use in metal-insulator-metal (MIM) capacitors, in an attempt to achieve a large cell capacitance (~10 fF/cell), a low leakage current density ($J \leq 1\times10^{-7}$ A/cm^2) at the operating voltage (0.6 V), and a maximum processing temperature of less than 650°C beyond sub 20 nm technology node [18, 22, 23]. These properties are beneficial for DRAM applications. Atomic layer deposition (ALD) has typically been used to fabricate conformal films on three-dimensional structures, such as cylindrical devices with aspect ratios of greater than 30 [22, 23]. ZrO_2 dielectric-based MIM capacitors have been studied extensively because ZrO_2 has a high *k* value (20-40) and a large band gap ($E_g \approx 5.8$ eV) [18, 24-35]. To obtain large *k* values, ZrO_2 samples with tetragonal, orthorhombic, and cubic phases have been fabricated at high growth temperatures, followed by post-deposition annealing (PDA). Crystalline ZrO_2 exhibit a high leakage current (*J*) along its grain boundaries [24, 29]. To reduce *J*, a high-*k* interlayer can be inserted into the center of the ZrO_2 film, forming a ZrO_2/high-*k*/ZrO_2 nanolaminate insulating film. Al_2O_3 is typically employed as the high-*k* interlayer because of its amorphous structure and large E_g of 8.8 eV [8, 11, 27-30, 33-38]. However, the low *k* value of amorphous Al_2O_3 (6-9) increases the capacitance equivalent thickness (CET) of the overall insulating film [8, 24]. Moreover, it remains unclear how the amorphous structure and E_g of the high-*k* interlayer affect the *J* characteristics of ZrO_2/high-*k*/ZrO_2.

The present study investigates several high-*k* materials for use as interlayers. $(Ta/Nb)O_x$ (TN) has a high *k* value of ~29, an amorphous structure at high process temperatures (~600°C), and a low E_g (4.4 eV) [8, 34, 35]. A $(Ta/Nb)O_x$-Al_2O_3 (TNA) nanolaminate is expected to exhibit an increased E_g compared to that for the TN interlayer and a reduced CET compared to that of Al_2O_3.

In this study, we investigated the effect of high-*k* interlayers of Al_2O_3, TN, and TNA on the CET and *J* properties of DRAM capacitors with TiN electrodes. We discuss how the amorphous structure and the conduction band energy (E_c) for the high-*k* interlayer affect the final electrical properties.

2. Experimental

The MIM capacitors with ZrO_2/high-*k*/ZrO_2 nanolaminate insulating films consisted of a TiN top electrode (BE-TiN), a 1st ZrO_2 layer, a high-*k* interlayer, a 2nd ZrO_2 layer, and TiN top electrodes (TE-TiN), as shown in Fig. 1. The 15-nm-thick BE-TiN was deposited on a SiO_2/p-Si substrate by DC sputtering. The 3.8-nm-thick 1st ZrO_2 layer was deposited on the BE-TiN by ALD at 300°C using $(C_5H_5)Zr[N(CH_3)_2]_3$ as the precursor and H_2O as the gas. Three different high-*k* interlayers, *viz*., Al_2O_3, TN, and TNA, were prepared. Al_2O_3 and TN layers were deposited by ALD at 200°C by using $Al(CH_3)_3$ and a (Ta/Nb = 1/1) $(NtAm)(NMe_2)_3$ cocktail precursor, respectively, and H_2O as the gas. The TNA nanolaminate layers were fabricated by alternate deposition cycles of TN and Al_2O_3. The thickness of the high-*k* interlayer was varied from 0.1 to 1.1 nm by changing the number of ALD cycles. The 3.8-nm-thick 2nd ZrO_2 layer was then deposited under the same ALD conditions as the 1st ZrO_2 layer. The thicknesses of all ZrO_2/high-*k*/ZrO_2 insulating layers are tabulated in Table I. PDA was carried out at 600°C for 30 s in an O_2 atmosphere. A 100-nm-thick TE-TiN film was then fabricated on the insulating film by photolithography, DC sputtering, and a liftoff process. The area of each square TE-TiN was approximately 4.0×10^{-6} cm^2. TiN/ZrO_2/TiN capacitors with a ZrO_2 thickness of 7.6-12.6 nm were also prepared as a reference.

The thicknesses of the ZrO_2, Al_2O_3, TN, and TNA layers were measured using spectroscopic ellipsometry. The film roughness was evaluated by atomic force microscopy (AFM). The crystal structure of the ZrO_2 films was analyzed by X-ray diffraction (XRD). Capacitance-voltage (*C*-*V*) and current-voltage (*I*-*V*) measurements were carried out at room temperature under ambient conditions using an Agilent B1500A semiconductor device analyzer and a Keithley 4200-SCS semiconductor characterization system, respectively. *C*-*V* measurements were performed in the range of −1.0 to 1.0 V at a frequency of 100 kHz. The CET was calculated as $3.9\varepsilon_0 A/C$, where 3.9, ε_0, A, and C are the *k* value for SiO_2, the vacuum permittivity, the capacitor area, and the capacitance of the insulating films, respectively, the latter of which was determined from the *C*-*V* characteristics at a voltage of 0 V.

3. Results and discussion

3.1 Characteristics of ZrO_2/high-k/ZrO_2 nanolaminate films

Figure 2 shows the dependence of the film thickness on the number of ALD cycles for as-grown and PDA-treated (a) ZrO_2 films and (b) Al_2O_3, TN, and TNA films employed as high-*k* interlayers. An almost ideal linear relationship between the numbers of ALD cycles and the thickness of the as-grown ZrO_2 film and high-*k* interlayers was achieved even for extremely thin films, which is indicative of a highly controlled deposition process. The growth rates for the as-grown ZrO_2, Al_2O_3, TN, and TNA films, obtained from the slopes of the linear fits, were 0.043, 0.114, 0.074, and 0.094 nm/cycle, respectively. For the PDA-treated films, the corresponding growth rates were 0.042, 0.106, 0.066, and 0.087 nm/cycle, which are 2-12% lower than those for the as-grown films. This is due to the densification of the films during the PDA process [39, 40].

A cross-sectional TEM image of a PDA-treated MIM capacitor with a ZrO_2/(Ta/Nb)O_x-Al_2O_3/ZrO_2 (ZTNAZ) multilayer structure is shown in Fig. 3(a). The thicknesses of the 1st ZrO_2, TNA, and 2nd ZrO_2 layers were 3.8, 0.9, and 3.8 nm, respectively. The polycrystalline nature of the ZrO_2 layers is evident from the lattice fringes with different orientations. It can be seen that all of the layers appear uniformly thick and the interfaces are sharp. Therefore, we confirmed that the 0.9-nm-thick TNA interlayer with an amorphous structure was well deposited between 1st and 2nd ZrO_2 layers, clearly separating them.

ZrO_2 typically forms four phases, such as monoclinic (m-ZrO_2), tetragonal (t-ZrO_2), orthorhombic (o-ZrO_2), and cubic phases (c-ZrO_2) [41, 42]. According to the Clausius-Mossotti relation, the *k* value for ZrO_2 increases with its density. Therefore, t-, o-, and c-ZrO_2 are preferable to m-ZrO_2 for use as the insulating layer in DRAM capacitors. The static *k* values for m-, t-, and c-ZrO_2 have been reported to be 19.7, 46.6, and 36.8, respectively [43, 44].

The crystal structure of the ZrO_2 and ZTNAZ films was investigated using XRD. Figure 3(b) shows XRD patterns for PDA-treated MIM capacitors with ZrO_2 (7.6-nm thick) and ZTNAZ insulating films. In the latter case, the thickness of the 1st and 2nd ZrO_2 layers was 3.8 nm, and the thickness of the TNA layer was 0.9 nm. A strong peak is observed at about $2\theta = 30.5°$ for the ZrO_2 film, which can be assigned to t-, o-, or c-ZrO_2. The exact crystal structure is difficult to identify because the peak positions are too similar [25, 32]. The ZTNAZ film exhibits an XRD pattern similar to that for the ZrO_2 film. This indicates that both ZrO_2 layers in this multilayer film are also predominantly t-, o-, or c-ZrO_2, which have a higher *k* value than m-ZrO_2 ($2\theta = 28.2°$ and 31.5°).

Figure 4 shows AFM images and root-mean-square (RMS) roughness values for a 15-nm-thick BE-TiN film, and for ZrO_2, $ZrO_2/Al_2O_3/ZrO_2$ (ZAZ), $ZrO_2/(Ta/Nb)O_x/ZrO_2$ (ZTNZ), and ZTNAZ films. The multilayer films all had a CET of 1.1 nm following PDA. The RMS roughness value for the ZrO_2 film is comparable to that for the BE-TiN because very smooth surfaces were obtained even for crystalline ZrO_2 samples [45]. Therefore, the small RMS values of about 1.0 nm are remained even after fabrication of the ZAZ, ZTNZ, and ZTNAZ multilayer films.

3.2 Electrical properties of ZrO_2/high-k/ZrO_2 nanolaminate films

Figure 5(a) shows the *k* and CET values for the ZrO_2, ZAZ, ZTNZ, and ZTNAZ films used in the MIM capacitors. The *k* value for the 7.6-nm-thick ZrO_2 single layer is approximately 28. This high *k* value is thought to be associated with t-, o-, and c-ZrO_2, rather than m-ZrO_2, as is evident from Fig. 3(b). A *k* value of approximately 27-28 is observed for ZAZ when the thickness of the Al_2O_3 interlayer is < 0.4 nm. For Al_2O_3 interlayers with a thickness of 0.4 nm or more, the *k* value for ZAZ decreases linearly with increasing Al_2O_3 thickness. The *k* value for ZTNZ and ZTNAZ remains above 26, even for thick TN (0.8 nm) and TNA (0.7 nm) layers. For any given interlayer thickness, the CET increases in the order ZTNZ < ZTNAZ < ZAZ. This indicates that the CET for the multilayer film can be improved by using TN and TNA interlayers rather than Al_2O_3. Figure 5(b) shows the dependence of the CET for ZAZ, ZTNZ, and ZTNAZ on the interlayer thickness in the range 0.3-1.1 nm. The *k* values for Al_2O_3, TNA, and TN, which were estimated from the inverse of the slope of the linear fits, are approximately 6, 9, and 11, respectively. These values are lower than those for the bulk material because the high-*k* interlayers are only one or two unit cells thick.

Figure 6 shows the *J-V* characteristics of MIM capacitors with ZAZ, ZTNZ, and ZTNAZ insulating films. The *J* properties of ZTNZ did not improve upon inserting a 0.8-nm-thick TN interlayer compared to the others. However, the *J* values for ZTNAZ with a 0.4-nm-thick TNA interlayer were lower by up to two orders of magnitude than those for ZAZ and ZTNZ with the same CET of 1.1 nm. Increasing the CET from 1.1 to 1.2 nm drastically improved the *J* characteristics of ZAZ, indicating that the useful thickness of the Al_2O_3 interlayer at low *J* was more than 0.4 nm.

Figure 7 shows the relationship between CET and *J* at 0.6 V for MIM capacitors with ZrO_2, ZAZ, ZTNZ, and ZTNAZ insulating films. The ZTNZ capacitors exhibit high *J* values (> 10^{-5} A/cm^2). The *J* value for ZAZ decreases as the thickness of the Al_2O_3 interlayer increases beyond 0.4 nm (CET > 1.15 nm), which becomes lower than that for ZrO_2. The thickness of an Al_2O_3 monolayer is about 0.4 nm. Therefore, when the thickness of the Al_2O_3 interlayer is less than 0.4 nm, the Al_2O_3 interlayer could exhibit island formation, which results in the high J values. Thus, the J-V characteristics for ZAZ improve by inserting an Al_2O_3 monolayer between the ZrO_2 layers. Low J values (10^{-8}-10^{-7} A/cm^2) are obtained for ZTNAZ, with a 0.4-nm-thick TNA layer exhibiting the lowest value of 6.9×10^{-8} A/cm^2 for a CET of 1.1 nm. To obtain a similar J value, the CET for the ZrO_2 and ZAZ capacitors would have to be 1.7 and 1.2 nm, respectively. Furthermore, the J characteristics for ZTNAZ were better than those for ZAZ in the low-CET region because of the large thickness of the TNA interlayer relative to that of the Al_2O_3 interlayer. Thus, TNA is promising as a high-k interlayer material for future DRAM capacitors.

Here, we propose two reasons for the difference in the J-V characteristics of the different samples. One is the large value of the E_c for the high-k interlayer, which plays an important role in suppressing the J value. It has been reported that E_c increases by about 0.5 eV upon insertion of a 0.5-nm-thick Al_2O_3 layer between two ZrO_2 layers [33]. This means that the E_c for the high-k material is influenced by the insertion of a high-k interlayer with a thickness of less than 1 nm. Thus, the high J values for ZTNZ are due to a reduction in E_c for the overall film, which incorporates a TN layer whose E_c is lower than that for ZrO_2. On the other hand, the E_g for TNA is expected to increase relative to that for TN because the E_g values for layer-by-layer-deposited $(HfO_2)_x(Al_2O_3)_{1-x}$ films reportedly increased linearly with the number of Al_2O_3 layers, which have a larger E_g than that for HfO_2 [46]. Moreover, we assume that the TNA layer has a more stable amorphous structure than TN because Al_2O_3 remains amorphous even after annealing at temperatures of up to 900°C, while TN remains amorphous only up to 600°C. Thus,

Al_2O_3 and TNA interlayers increase the E_c for the overall insulating film and reduce the J value relative to that for a single layer of ZrO_2. The other criterion is the thickness of the high-k interlayer. The ZAZ insulating film incorporating an Al_2O_3 layer with a thickness of more than 0.4 nm exhibits lower J values than a single layer of ZrO_2. The J value for the ZTNAZ insulating film with a 0.4-nm-thick TNA layer is significantly reduced, whereas ZTNZ insulating films exhibit high J values regardless of the TN thickness. Thus, the high-k interlayer material needs to have a larger E_c than TN and a thickness of over 0.4 nm.

4. Conclusion

The characteristics of MIM capacitors with ZrO_2, ZAZ, ZTNZ, and ZTNAZ insulating films, which were fabricated by ALD and PDA, were studied systematically. The CET for the MIM capacitors increased in the order ZTNZ < ZTNAZ < ZAZ as a result of the k values of the Al_2O_3 (~6), TNA (~9) and TN (~11) high-k interlayers. ZTNAZ exhibited a lower J value (6.9×10^{-8} A/cm^2 at 0.6 V) than ZrO_2, ZAZ, and ZTNZ, all of which had a CET of 1.1 nm. These results indicated that the E_c, thickness, and amorphous structure of the high-k interlayer are important factors determining the J values of ZrO_2/high-k/ZrO_2 insulating films. The TNA nanolaminate layer is a promising high-k interlayer material for use in future DRAM capacitors.

Acknowledgments

This study was supported by the World Premier International Research Center Initiative (WPI) and the Ministry of Education, Culture, Sports, Science and Technology

(MEXT), and was partly supported by CREST, JST. The authors thank all staff members of the MANA Foundry, WPI-MANA, and NIMS for their support in fabricating the TiN/ZrO_2/high-*k*/ZrO_2/TiN MIM capacitors.

References

[1] J.A. Kittl, K. Opsomer, M. Popovici, N. Menou, B. Kaczer, X.P. Wang, C. Adelmann, M.A. Pawlak, K. Tomida, A. Rothschild, B. Govoreanu, R. Degraeve, M. Schaekers, M. Zahid, A. Delabie, J. Meersschaut, W. Polspoel, S. Clima, G. Pourtois, W. Knaepen, C. Detavernier, V.V. Afanas'ev, T. Blomberg, D. Pierreux, J. Swerts, P. Fischer, J.W. Maes, D. Manger, W. Vandervorst, T. Conard, A. Franquet, P. Favia, H. Bender, B. Brijs, S. Van Elshocht, M. Jurczak, J. Van Houdt, D.J. Wouters, High-*k* dielectrics for future generation memory devices, Microelectron. Eng. 86 (2009) 1789–1795.

[2] J. Robertson, R.M. Wallace, High-K materials and metal gates for CMOS applications, Mater. Sci. Eng. R 88 (2015) 1–41.

[3] G. He, L. Zhu, Z. Sun, Q. Wan, L. Zhang, Integrations and challenges of novel high-*k* gate stacks in advanced CMOS technology, Prog. Mater. Sci. 56 (2011) 475–572.

[4] G. He, X. Chen, Z. Sun, Interface engineering and chemistry of Hf-based high-k dielectrics on III–V substrates, Surf. Sci. Rep. 68 (2013) 68–107.

[5] G. He, J. Liu, H. Chen, Y. Liu, Z. Sun, X. Chen, M. Liu, L. Zhang, Interface control and modification of band alignment and electrical properties of HfTiO/GaAs gate stacks by nitrogen incorporation, J. Mater. Chem. C 2 (2014) 5299–5308.

[6] J.W. Zhang, G. He, L. Zhou, H.S. Chen, X.S. Chen, X.F. Chen, B. Deng, J.G. Lv, Z.Q. Sun, Microstructure optimization and optical and interfacial properties modulation of sputtering-derived HfO_2 thin films by TiO_2 incorporation, J. Alloys Compd. 611 (2014) 253–259.

[7] G. He, J. Gao, H. Chen, J. Cui, Z. Sun, X. Chen, Modulating the Interface Quality and Electrical Properties of HfTiO/InGaAs Gate Stack by Atomic-Layer-Deposition-Derived Al_2O_3 Passivation Layer, ACS Appl. Mater. Interfaces 6 (2014) 22013–22025.

[8] T. Nabatame, A. Ohi, K. Ito, M. Takahashi, T. Chikyo, Role of the $(Ta/Nb)O_x/Al_2O_3$ interface on the flatband voltage shift for $Al_2O_3/(Ta/Nb)O_x/Al_2O_3$ multilayer charge trap capacitors, J. Vac. Sci. Technol. A 33 (2015) 01A118.

[9] L. Alekseeva, T. Nabatame, T. Chikyow, A. Petrov, Resistive switching characteristics in memristors with Al_2O_3/TiO_2 and TiO_2/Al_2O_3 bilayers, Jpn. J. Appl. Phys. 55 (2016) 08PB02.

[10] K. Kurishima, T. Nabatame, M. Shimizu, N. Mitoma, T. Kizu, S. Aikawa, K. Tsukagoshi, A. Ohi, T. Chikyow, A. Ogura, Influence of Al_2O_3 layer insertion on the electrical properties of Ga-In-Zn-O thin-film transistors, J. Vac. Sci. Technol. A 33 (2015) 061506.

[11] T. Sawada, T. Nabatame, T.D. Dao, I. Yamamoto, K. Kurishima, T. Onaya, A. Ohi, K. Ito, M. Takahashi, K. Kohama, T. Ohishi, A. Ogura, T. Nagao, Improvement of smooth surface of RuO_2 bottom electrode on Al_2O_3 buffer layer and characteristics of $RuO_2/TiO_2/Al_2O_3/TiO_2/RuO_2$ capacitors, J. Vac. Sci. Technol. A 35 (2017) 061503.

[12] C. Wenger, M. Lukosius, H.J. Müssig, G. Ruhl, S. Pasko, C. Lohe, Influence of the electrode material on HfO_2 metal-insulator-metal capacitors, J. Vac. Sci. Technol. B 27 (2009) 286–289.

[13] F.E. Kamel, P. Gonon, C. Vallée, C. Jorel, Electrode effects on the conduction mechanisms in HfO_2-based metal-insulator-metal capacitors, J. Appl. Phys. 106 (2009) 064508.

[14] H. Hu, C. Zhu, Y.F. Lu, M.F. Li, B.J. Cho, W.K. Choi, A High Performance MIM Capacitor Using HfO_2 Dielectrics, IEEE Electron Device Lett. 23 (2002) 514–516.

[15] M. Lukosius, C.B. Kaynak, S. Kubotsch, T. Blomberg, G. Ruhl, C. Wenger, Properties of atomic-vapor and atomic-layer deposited Sr, Ti, and Nb doped Ta_2O_5 Metal–Insulator–Metal capacitors, Thin Solid Films 520 (2012) 4576–4579.

[16] P.C. Joshi, M.W. Cole, Influence of postdeposition annealing on the enhanced structural and electrical properties of amorphous and crystalline Ta_2O_5 thin films for dynamic random access memory applications, J. Appl. Phys. 86 (1999) 871–880.

[17] Y. Matsui, M. Hiratani, S. Kimura, I. Asano, Combining Ta_2O_5 and Nb_2O_5 in Bilayered Structures and Solid Solutions for Use in MIM Capacitors, J. Electrochem. Soc. 152 (2005) F54–F59.

[18] M. Pešić, S. Knebel, M. Geyer, S. Schmelzer, U. Böttger, N. Kolomiiets, V.V. Afanas'ev, K. Cho, C. Jung, J. Chang, H. Lim, T. Mikolajick, U. Schroeder, Low leakage ZrO_2 based capacitors for sub 20 nm dynamic random access memory technology nodes, J. Appl. Phys. 119 (2016) 064101.

[19] M. Popovici, J. Swerts, A. Redolfi, B. Kaczer, M. Aoulaiche, I. Radu, S. Clima, J.L. Everaert, S.V. Elshocht, M. Jurczak, Low leakage Ru-strontium titanate-Ru metal-insulator-metal capacitors for sub-20 nm technology node in dynamic random access memory, Appl. Phys. Lett. 104 (2014) 082908.

[20] B. Kaczer, S. Clima, K. Tomida, B. Govoreanu, M. Popovici, M.S. Kim, J. Swerts, A. Belmonte, W.C. Wang, V.V. Afanas'ev, A.S. Verhulst, G. Pourtois, G. Groeseneken, M. Jurczak, Considerations for further scaling of metal–insulator–metal DRAM capacitors, J. Vac. Sci. Technol. B 31 (2013) 01A105.

[21] G.J. Choi, S.K. Kim, S.Y. Lee, W.Y. Park, M. Seo, B.J. Choi, C.S. Hwang, Atomic Layer Deposition of TiO_2 Films on Ru Buffered TiN Electrode for Capacitor Applications, J. Electrochem. Soc. 156 (2009) G71–G77.

[22] S.K. Kim, K.M. Kim, D.S. Jeong, W. Jeon, K.J. Yoon, C.S. Hwang, Titanium dioxide thin films for next-generation memory devices, J. Mater. Res. 28 (2013) 313–325.

[23] S.K. Kim, G.J. Choi, S.Y. Lee, M. Seo, S.W. Lee, J.H. Han, H.S. Ahn, S. Han, C.S. Hwang, Al-Doped TiO_2 Films with Ultralow Leakage Currents for Next Generation DRAM Capacitors, Adv. Mater. 20 (2008) 1429–1435.

[24] S. Knebel, M. Pešić, K. Cho, J. Chang, H. Lim, N. Kolomiiets, V.V. Afanas'ev, U. Muehle, U. Schroeder, T. Mikolajick, Ultra-thin ZrO_2/SrO/ZrO_2 insulating stacks for future dynamic random access memory capacitor applications, J. Appl. Phys. 117 (2015) 224102.

[25] D.C. Won, S.W. Rhee, Effect of process temperature on the structural and electrical properties of atomic layer deposited ZrO_2 films using tris(dimethylamino) cyclopentadienyl zirconium precursor, J. Vac. Sci. Technol. B 32 (2014) 03D102.

[26] Y. Kiyota, K. Itaka, Y. Iwashita, T. Adachi, T. Chikyow, A. Ogura, Combinatorial Investigation of ZrO_2-Based Dielectric Materials for Dynamic Random-Access Memory Capacitors, Jpn. J. Appl. Phys. 50 (2011) 06GH12.

[27] W. Weinreich, A. Shariq, K. Seidel, J. Sundqvist, A. Paskaleva, M. Lemberger, A.J. Bauer, Detailed leakage current analysis of metal–insulator–metal capacitors with ZrO_2, ZrO_2/SiO_2/ZrO_2, and ZrO_2/Al_2O_3/ZrO_2 as dielectric and TiN electrodes, J. Vac. Sci. Technol. B 31 (2013) 01A109.

[28] D. Panda, T.Y. Tseng, Growth, dielectric properties, and memory device applications of ZrO_2 thin films, Thin Solid Films 531 (2013) 1–20.

[29] D. Martin, M. Grube, W. Weinreich, J. Müller, W.M. Weber, U. Schröder, H. Riechert, T. Mikolajick, Mesoscopic analysis of leakage current suppression in $ZrO_2/Al_2O_3/ZrO_2$ nano-laminates, J. Appl. Phys. 113 (2013) 194103.

[30] H.J. Cho, Y.D. Kim, D.S. Park, E. Lee, C.H. Park, J.S. Jang, K.B. Lee, H.W. Kim, Y.J. Ki, I.K. Han, Y.W. Song, New TIT capacitor with $ZrO_2/Al_2O_3/ZrO_2$ dielectrics for 60 nm and below DRAMs, Solid-State Electron. 51 (2007) 1529–1533.

[31] J.H. Kim, V. Ignatova, P. Kücher, J. Heitmann, L. Oberbeck, U. Schröder, Physical and electrical characterization of high-*k* ZrO_2 metal–insulator–metal capacitor, Thin Solid Films 516 (2008) 8333–8336.

[32] S.K. Kim, C.S. Hwang, Atomic Layer Deposition of ZrO_2 Thin Films with High Dielectric Constant on TiN Substrates, Electrochem. Solid State Lett. 11 (2008) G9–G11.

[33] S.Y. Lee, J. Chang, Y. Kim, H. Lim, H. Jeon, H. Seo, Depth resolved band alignments of ultrathin TiN/ZrO_2 and TiN/ZrO_2-Al_2O_3-ZrO_2 dynamic random access memory capacitors, Appl. Phys. Lett. 105 (2014) 201603.

[34] S. Miyazaki, Photoemission study of energy-band alignments and gap-state density distributions for high-*k* gate dielectrics, J. Vac. Sci. Technol. B 19 (2001) 2212–2216.

[35] J. Robertson, Band offsets of wide-band-gap oxides and implications for future electronic devices, J. Vac. Sci. Technol. B 18 (2000) 1785–1791.

[36] M.Y. Li, B.S. Tsai, P.C. Jiang, H.C. Wu, Y.H. Wu, Y.J. Lin, Structure and property changes of $ZrO_2/Al_2O_3/ZrO_2$ laminate induced by low-temperature NH_3 annealing applicable to metal–insulator–metal capacitor, Thin Solid Films 518 (2010) 5272–5277.

[37] D. Zhou, U. Schroeder, J. Xu, J. Heitmann, G. Jegert, W. Weinreich, M. Kerber, S. Knebel, E. Erben, T. Mikolajick, Reliability of Al_2O_3-doped ZrO_2 high-*k* dielectrics in three-dimensional stacked metal-insulator-metal capacitors, J. Appl. Phys. 108 (2010) 124104.

[38] Y.H. Wu, C.K. Kao, B.Y. Chen, Y.S. Lin, M.Y. Li, H.C. Wu, High density metal-insulator-metal capacitor based on $ZrO_2/Al_2O_3/ZrO_2$ laminate dielectric, Appl. Phys. Lett. 93 (2008) 033511.

[39] H.S. Jung, J.H. Jang, D.Y. Cho, S.H. Jeon, H.K. Kim, S.Y. Lee, C.S. Hwang, The Effects of Postdeposition Annealing on the Crystallization and Electrical Characteristics of HfO_2 and ZrO_2 Gate Dielectrics, Electrochem. Solid State Lett. 14 (2011) G17–G19.

[40] S. Jakschik, U. Schroeder, T. Hecht, M. Gutsche, H. Seidl, J.W. Bartha, Crystallization behavior of thin ALD-Al_2O_3 films, Thin Solid Films 425 (2003) 216–220.

[41] C.R. Babu, N.R.M. Reddy, K. Reddy, Synthesis and characterization of high dielectric nano zirconium oxide , Ceramics International 41 (2015) 10675–10679.

[42] M. Sternik, K. Parlinski, Lattice vibrations in cubic, tetragonal, and monoclinic phases of ZrO_2, J. Chem. Phys. 122 (2005) 064707.

[43] D. Vanderbilt, X. Zhao, D. Ceresoli, Structural and dielectric properties of crystalline and amorphous ZrO_2, Thin Solid Films 486 (2005) 125–128.

[44] X. Zhao, D. Vanderbilt, Phonons and lattice dielectric properties of zirconia, Phys. Rev. B 65 (2002) 075105.

[45] V. Yanev, M. Rommel, M. Lemberger, S. Petersen, B. Amon, T. Erlbacher, A.J. Bauer, H. Ryssel, A. Paskaleva, W. Weinreich, C. Fachmann, J. Heitmann, U. Schroeder, Tunneling atomic-force microscopy as a highly sensitive mapping tool for the

characterization of film morphology in thin high-*k* dielectrics, Appl. Phys. Lett. 92 (2008) 252910.

[46] H.Y. Yu, M.F. Li, B.J. Cho, C.C. Yeo, M.S. Joo, D.L. Kwong, J.S. Pan, C.H. Ang, J.Z. Zheng, S. Ramanathan, Energy gap and band alignment for $(HfO_2)_x(Al_2O_3)_{1-x}$ on (100) Si, Appl. Phys. Lett. 81 (2002) 376–378.

Table Captions

Table 1. Specifications of MIM capacitors with ZrO_2/high-*k*/ZrO_2 insulating films.

ZrO_2/high-*k*/ZrO_2 insulating film	1st ZrO_2 layer (nm)	High-*k* interlayer (nm)	2nd ZrO_2 layer (nm)
ZAZ	3.8	0.1–1.1	3.8
ZTNZ	3.8	0.4, 0.8	3.8
ZTNAZ	3.8	0.4–0.9	3.8

Figure Captions

Fig. 1. Schematic of MIM capacitor with ZrO_2/high-*k*/ZrO_2 nanolaminate insulating film and TiN electrodes.

Fig. 2. Dependence of film thickness on number of ALD cycles for as-grown and PDA-treated (a) ZrO_2 film and (b) Al_2O_3, TN, and TNA films, which were used as high-*k* interlayers.

Fig. 3. (a) Cross-sectional TEM image of PDA-treated MIM capacitor with ZTNAZ insulating film. (b) XRD patterns of PDA-treated MIM capacitors with ZrO_2 (7.6 nm) and ZTNAZ insulating films. The thicknesses of the 1st ZrO_2, TNA, and 2nd ZrO_2 layers were 3.8, 0.9, and 3.8 nm, respectively.

Fig. 4. AFM images and RMS roughness values for PDA-treated (a) 15-nm-thick BE-TiN, (b) ZrO_2 (CET = 1.1 nm), (c) ZAZ (CET = 1.2 nm), (d) ZTNZ (CET = 1.1 nm), and (e) ZTNAZ (CET = 1.1 nm).

Fig. 5. (a) *k* and CET values for ZrO_2, ZAZ, ZTNZ, and ZTNAZ insulating films used in MIM capacitors. (b) CET values for ZAZ, ZTNZ, and ZTNAZ insulating films in MIM capacitors as a function of the high-*k* interlayer thickness in the thickness range of 0.3-1.1 nm. The *k* values for the interlayers were estimated from the inverse of the slope of the linear fits.

Fig. 6. *J*-*V* characteristics of MIM capacitors with ZAZ, ZTNZ, and ZTNAZ insulating films.

Fig. 7. Relationship between CET and *J* at 0.6 V for MIM capacitors with ZrO_2, ZAZ, ZTNZ, and ZTNAZ insulating films.

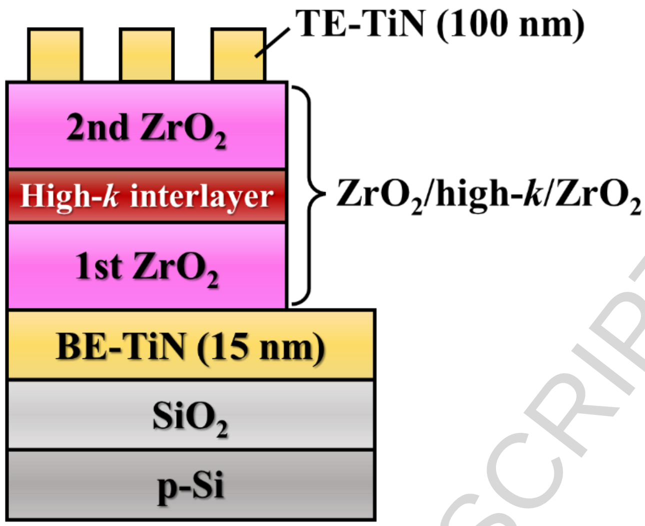
TE-TiN (100 nm)
2nd ZrO_2
High-*k* interlayer
1st ZrO_2
ZrO_2/high-*k*/ZrO_2
BE-TiN (15 nm)
SiO_2
p-Si

Fig. 1

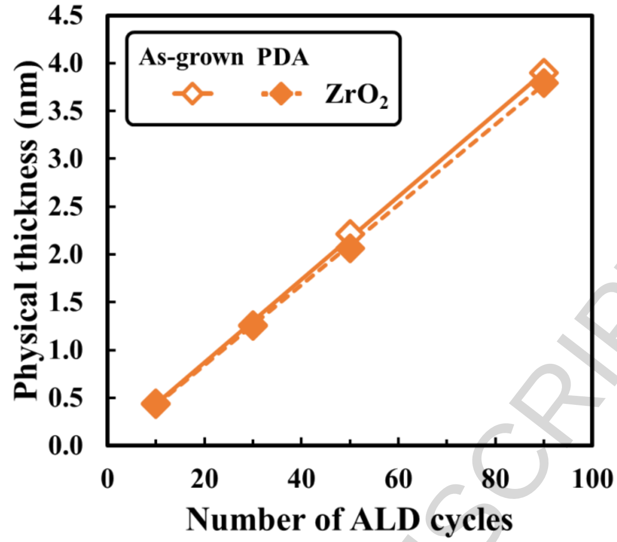
As-grown PDA
ZrO2
Physical thickness (nm)
4.5
4.0
3.5
3.0
2.5
2.0
1.5
1.0
0.5
0.0
0
20
40
60
80
100
Number of ALD cycles

Fig. 2 (a)

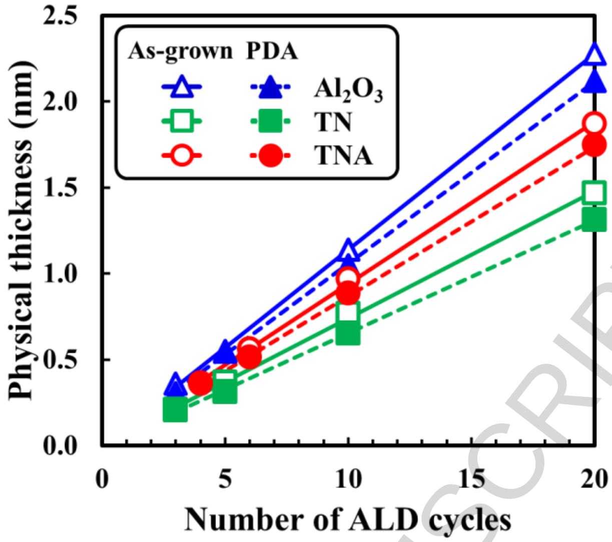

As-grown PDA
Al2O3
TN
TNA
Physical thickness (nm)
2.5
2.0
1.5
1.0
0.5
0.0
0
5
10
15
20
Number of ALD cycles

Fig. 2 (b)

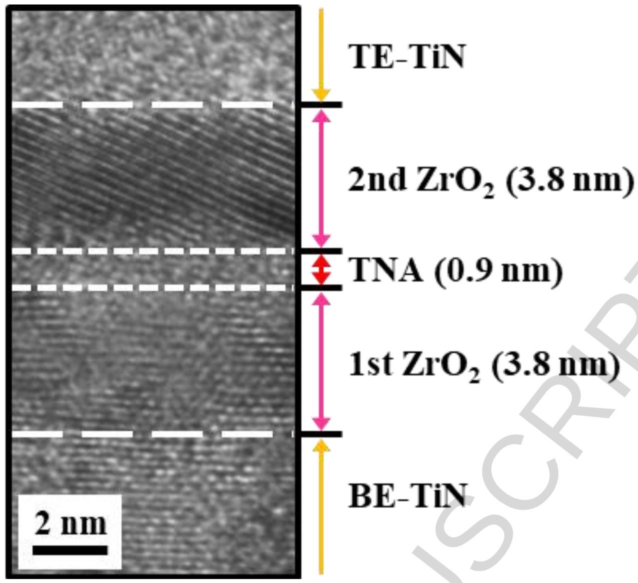

Fig. 3 (a)

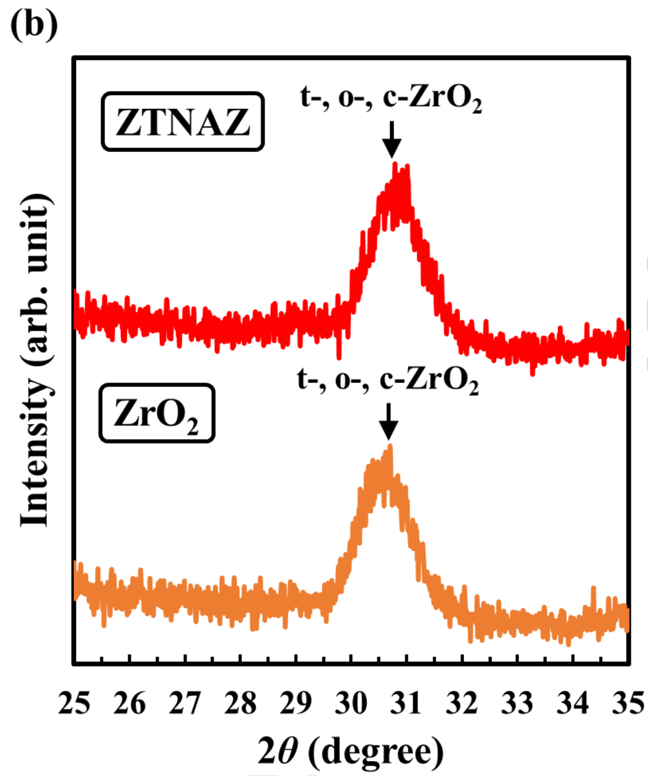
(b)
ZTNAZ
t-, o-, c-ZrO2
ZrO2
t-, o-, c-ZrO2
Intensity (arb. unit)
25 26 27 28 29 30 31 32 33 34 35
2θ (degree)

Fig. 3 (b)

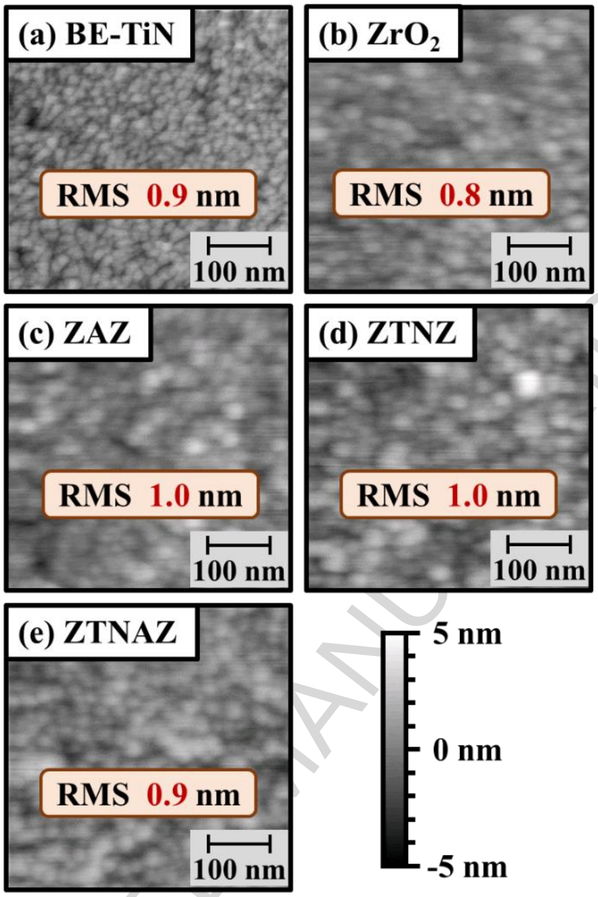
(a) BE-TiN
RMS 0.9 nm
100 nm
(b) ZrO_2
RMS 0.8 nm
100 nm
(c) ZAZ
RMS 1.0 nm
100 nm
(d) ZTNZ
RMS 1.0 nm
100 nm
(e) ZTNAZ
RMS 0.9 nm
100 nm
5 nm
0 nm
-5 nm

Fig. 4

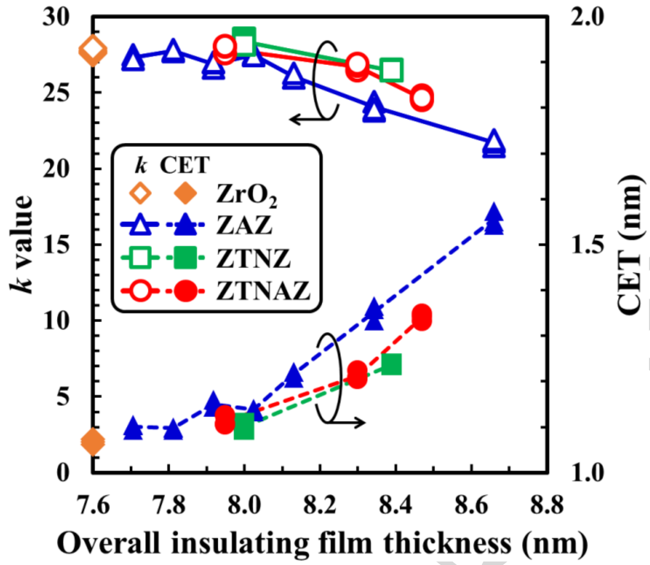
k value
CET (nm)
Overall insulating film thickness (nm)
k CET
ZrO2
ZAZ
ZTNZ
ZTNAZ
30
25
20
15
10
5
0
2.0
1.5
1.0
7.6
7.8
8.0
8.2
8.4
8.6
8.8

Fig. 5 (a)

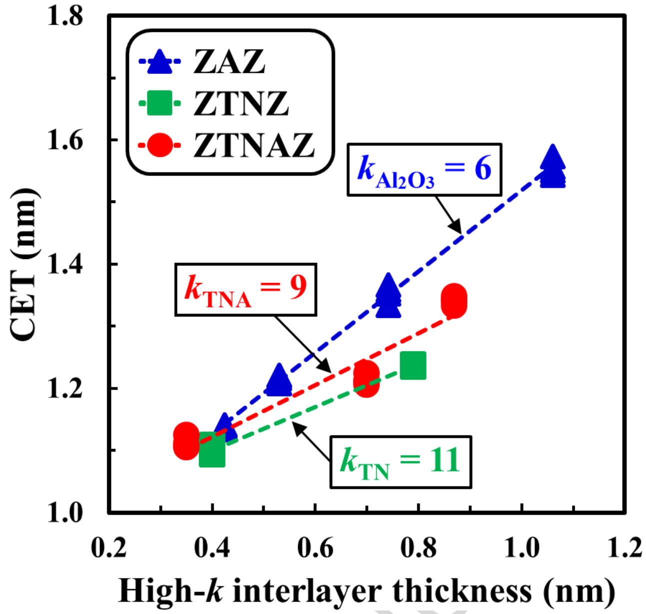
1.8
1.6
1.4
1.2
1.0
CET (nm)
0.2
0.4
0.6
0.8
1.0
1.2
High-k interlayer thickness (nm)
ZAZ
ZTNZ
ZTNAZ
k_Al2O3 = 6
k_TNA = 9
k_TN = 11

Fig. 5 (b)

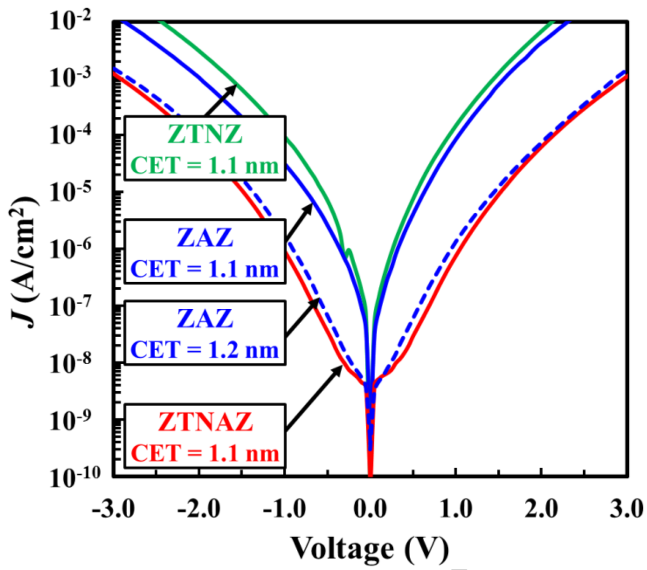

10-2
10-3
10-4
10-5
10-6
10-7
10-8
10-9
10-10
J (A/cm2)
-3.0
-2.0
-1.0
0.0
1.0
2.0
3.0
Voltage (V)
ZTNZ
CET = 1.1 nm
ZAZ
CET = 1.1 nm
ZAZ
CET = 1.2 nm
ZTNAZ
CET = 1.1 nm

Fig. 6

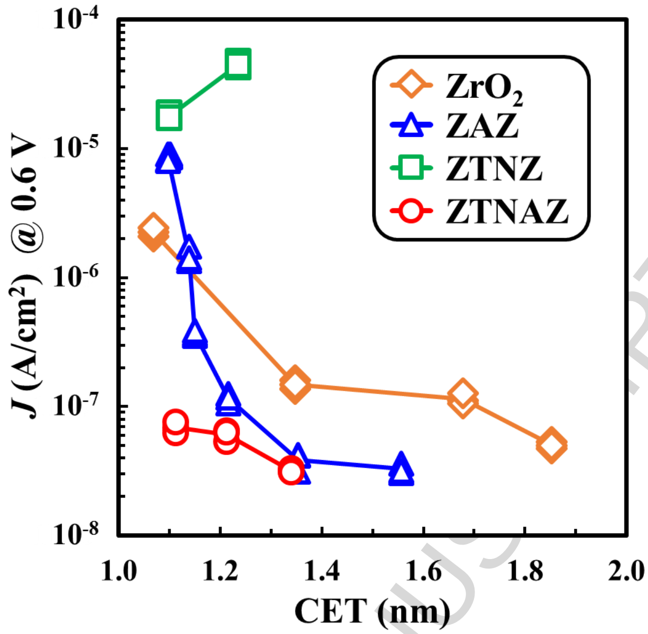

10-4
10-5
10-6
10-7
10-8
J (A/cm2) @ 0.6 V
1.0
1.2
1.4
1.6
1.8
2.0
CET (nm)
ZrO2
ZAZ
ZTNZ
ZTNAZ

Fig. 7

Highlights

- We investigated characteristics of ZrO_2/high-*k*/ZrO_2 nanolaminate insulating films.
- Al_2O_3, $(Ta/Nb)O_x$ (TN), and TN-Al_2O_3 (TNA) layers were prepared as high-*k* interlayers.
- The CET value of the MIM capacitors increased in the order ZTNZ < ZTNAZ < ZAZ.
- The *J* value at 0.6 V with a CET of 1.1 nm increased in the order ZTNAZ < ZAZ < ZTNZ.
- TNA is a promising high-*k* interlayer material for use in future DRAM capacitors.